Ceramics International 46 (2020) 9218–9224

Contents lists available at ScienceDirect

Ceramics International

journal homepage: www.elsevier.com/locate/ceramint

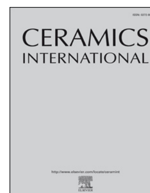

Quantitative investigation of electromechanical coupling of potassium sodium niobate-based thin films

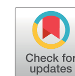

Lei Wang[a], Jihong Bian[a], Fei Shao[b], Bian Yang[a], Linglong Li[c], Zhongshuai Liang[d,e], Guohua Lan[d,e], Ming Liu[d,e], Junqi Gao[f,g,**], Yaodong Yang[a,e,*]

[a] Frontier Institute of Science and Technology, Xi'an Jiaotong University, Xi'an, 710049, China
[b] School of Materials Science and Engineering, University of Science and Technology Beijing, Beijing, 100083, China
[c] Department of Physics, Tsinghua University, Beijing, 100083, China
[d] School of Microelectronics, Xi'an Jiaotong University, Xi'an, 710049, China
[e] State Key Laboratory for Mechanical Behavior of Materials and School of Materials Science and Engineering, Xi'an Jiaotong University, Xi'an, 710049, China
[f] Acoustic Science and Technology Laboratory, Harbin Engineering University, Harbin, 150001, China
[g] College of Underwater Acoustic Engineering, Harbin Engineering University, Harbin, 150001, China

ARTICLE INFO

Keywords:
Lead-free
Piezoelectric thin films
Piezoresponse force microscopy
Machine learning

ABSTRACT

High-performance environment-friendly piezoelectric potassium sodium niobate (KNN)-based thin films have been emerged as promising lead-free candidates, while their substrate-dependent piezoelectricity faces the lack of high-quality information due to restraints in measurements. Although piezoresponse force microscopy (PFM) is a potential measuring tool, still its regular mode is not considered as a reliable characterization method for quantification. After combining machine-learning enabled analysis using PFM datasets, it is possible to measure piezoelectric properties quantitatively. Here we utilized advanced PFM technology empowered by machine learning to measure and compare the piezoelectricity of KNN based thin films on different substrates. The results provide a better understanding of the relationship between structures and piezoelectric properties of the thin films.

1. Introduction

At present, piezoelectric thin films have been widely applied in various electronic devices, such as integrated micro-sensors and small actuators [1–3]. Among many well-known piezoelectric materials, Pb$(Zr,Ti)O_3$-based thin films have been used broadly because of its superior piezoelectric performance [4–6]. Due to the concerns about environment and health issues, lead-based products have been forbidden from many commercial applications [7]. Therefore, the investigations of developing lead-free piezoelectric thin films with excellent performance have been attracting lots of interests recently. Several materials, such as $Ba(Zr_{0.2}Ti_{0.8})O_3$-$Ba_{0.7}Ca_{0.3}TiO_3$, $Na_{0.5}Bi_{0.5}TiO_3$, $(K, Na)NbO_3$ (KNN) etc., have been paid much attention [8–11]. KNN-based perovskite material is one of the promising candidates considering its high Curie temperature and received excellent piezoelectric properties after doping engineering [8,12]. It perceived that piezoelectric properties can be tuned greatly after elemental doping. For example, an ultrahigh piezoelectric coefficient of d_{33} = 416 pC/N has been achieved in (K, Na, Li) (Nb, Ta, Sb)O_3 ceramic [8]. Therefore, lots of researches have focused on doping engineering to enhance piezoelectric properties [9,13,14]. In addition to the doping engineering, the effect of substrates needs to be considered as well when depositing thin films on the top of them, as the strain originated from the lattice mismatch in between can strongly influence on the piezoelectric properties [15–18].

Considering the scales, unlike ceramic pellets thin films have quite different dimensions [19], which need new tools to precisely measure the properties and build up the relationships between the structures and piezoelectric coefficients of thin films. Piezoresponse force microscopy (PFM) is an efficient tool to detect local electromechanical properties at the nanoscale [20,21], but collection of correct data using PFM is still questionable. The conventional single-frequency (SF) PFM is difficult to deal with the probe-surface resonance frequency drift, which is mainly caused by the cross-talk between the surface morphology, static force and the electrochemical response. Therefore, the signal intensity or stability is hardly guaranteed during scanning. In other words, it is not accurate for single-frequency (SF) PFM to measure piezoelectricity

* Corresponding author. Frontier Institute of Science and Technology, Xi'an Jiaotong University, Xi'an, 710049, China.
** Corresponding author. Acoustic Science and Technology Laboratory, Harbin Engineering University, Harbin, 150001, China.
E-mail addresses: gaojunqi@hrbeu.edu.cn (J. Gao), yaodongy@xjtu.edu.cn (Y. Yang).

https://doi.org/10.1016/j.ceramint.2019.12.174
Received 2 November 2019; Received in revised form 2 December 2019; Accepted 21 December 2019
Available online 23 December 2019
0272-8842/ © 2019 Elsevier Ltd and Techna Group S.r.l. All rights reserved.

quantitatively [21]. Benefiting from exciting two frequencies on both sides of resonance peak, dual AC resonance tracking (DART) PFM has shown the capability of decreasing the influence of the resonance frequency drift [20,21]; while band excitation (BE) PFM further excites a band of frequency (including resonance frequency) [22–24]. Above mentioned both methods could be possible solutions to overcome the weakness of SF-PFM. But scientists are still looking for better technologies to measure piezoelectricity quantitatively.

With the rapid development of machine learning (ML) in the research of materials science, it conceived that mutual integration of the ML and PFM measurements provides an alternative technology for more precise studies of electromechanical materials [25–30]. For instance, unsupervised principle component analysis (PCA), a general algorithm for data dimension reduction, has been widely used in material science, such as understanding the phase transition of PMN-PT [27], quantitative study of the flexoelectricity in $PbTiO_3/SrTiO_3$ superlattice polar vortices [30], and measuring the electromechanical energy conversion in PZT thin films [26]. These prior successful experiences indicate that ML is a promising tool in scanning probe microscopy measurement. In this study, we provide a quantitative way to measure the piezoelectricity of thin films at the nanoscale with the support of ML.

To study the effect of substrate on piezoelectric properties of the lead-free KNN based thin films, we firstly used $0.96(K_{0.5}Na_{0.5})_{0.95}Li_{0.05}Nb_{0.93}Sb_{0.07}O_3$-$0.04BaZrO_3$ (KNLNS-BZ, reported bulk piezoelectric coefficient d_{33} is 425 pC/N) ceramics as a target to fabricate the thin films on three different substrates by pulsed laser deposition (PLD) [31,32]. The thin films with complex components are designed for the high piezoresponse inheritance from ceramics. Three representative substrates are used: 1. $LaAlO_3$, a normal perovskite substrate for epitaxial thin films; 2. miscut $SrTiO_3$, a perovskite substrate with 5° miscut; 3. Si, the most widely used substrate in industrial, is used for polycrystalline films growth. Four different atomic force microscopes characterization modes i.e. DART-PFM, BE-PFM, sequential excitation PFM (SE-PFM) [29], switching spectroscopy PFM (SS-PFM), are used to measure the local piezoelectricity quantitatively and build up both the intrinsic and extrinsic relationship between the microstructure and the piezoresponse properties.

2. Experimental section

KNLNS-BZ films were grown on LAO (100), STO (100) and Si substrates using pulsed laser deposition with a fourth-harmonic wave of an Nd:YAG laser. Before deposition, the chamber was evacuated to a base pressure of 10^{-7} mbar. During the deposition, the critical parameters were set up as following: deposition temperature was 700 °C; laser repetition rate was 3 Hz; laser energy density was 1.8 J/cm^2, and flowing oxygen pressure was 0.1 mbar. After deposition, the films were *in situ* annealed for 10 min under an oxygen pressure of 10 mbar, followed by cooling down to 300 °C with temperature decreasing rate of 10 °C/min and then cooled down to room temperature naturally.

Crystallographic properties were investigated firstly by high-resolution X-ray diffraction (HRXRD) using a PANalytical X'Pert MRD. Then, an Asylum Research Cypher AFM was used to perform the PFM measurements, including DART-PFM, build-in BE-PFM, SE-PFM, and SS-PFM. An AC bias with an amplitude of 0.8 V near the sample–probe resonance frequency applied to the KNLNS-BZ thin films to amplify the piezoresponse. An Asylum ASYELEC-01 tip with a spring constant of 2 Nm^{-1} was used during DART-PFM and BE-PFM scanning, and the bandwidth is set to 20 kHz in BE-PFM. To measure the SE-PFM, a series of single-frequency PFM mappings were acquired under an AC voltage of 0.8 V using an Olympus AC240TM with a spring constant of 2 Nm^{-1}. The distribution of resonance frequency (ω_0) over the scanned region is determined from a preliminary DART-PFM scan, so the adopted frequency range covers the resonance frequencies of all the points. Olympus AC240TM was also used to finish SS-PFM under a DC voltage ranging from −30 V to 30 V (with a high voltage module in the Cypher system) with a Triangle Square waveform, and all the samples were measured by 50 × 50 grid points in 3 μm × 3 μm regions and took the average of 10 chosen points in SS-PFM. In the same PFM method measurement, the laser spot position was calibrated and set to be the same.

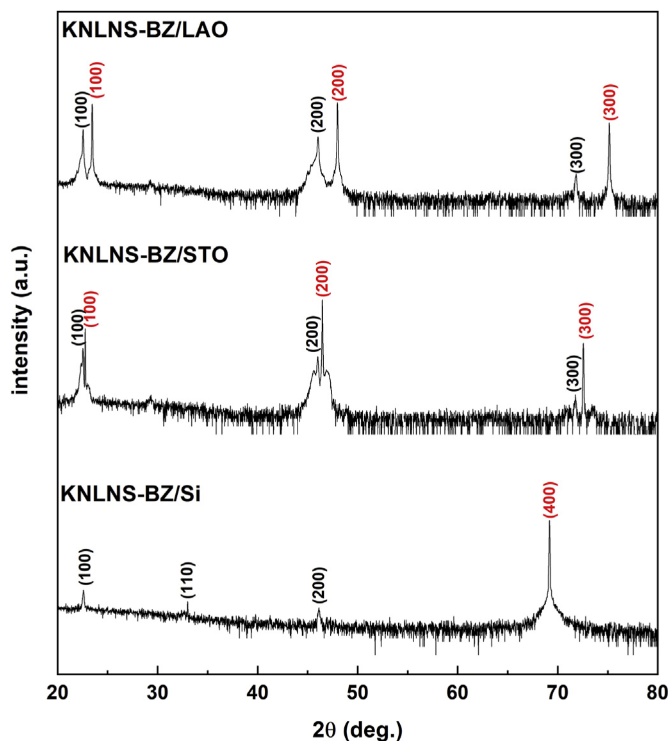

Fig. 1. XRD patterns of KNLNS-BZ thin films grown on three different substrates, the black labels indicate the thin film peaks and the red ones are from substrates. (For interpretation of the references to color in this figure legend, the reader is referred to the Web version of this article).

3. Results and discussion

Typical XRD line scan patterns of KNLNS-BZ thin films on different substrates are shown in Fig. 1. The films reveal pure perovskite structure without impurity phases. All three films correspond to tetragonal symmetry (T-phase), especially significant shoulder peak (45.6°) represents (002) peak with lower intensity on STO substrate, which is consistent with the standard diffraction peaks of KNN [32,33]. The results indicate that the doped Li, Sb, and others elements have completely been diffused into KNN lattice to form a solid solution. An interesting fact is that the corresponding KNLNS-BZ ceramic is in phase boundary between T-phase and orthorhombic (O) phase at room temperature while the films show pure T-phase owing to the influence of the strain from the substrates [32]. The films grown on LAO and STO substrates are (100) surface normal, even though the STO substrate is a 5° miscut substrate. This is coincident with the literature, due to the perovskite structures of the KNLNS-BZ, LAO and STO, while the Si has a diamond-like structure. The thin films were deposited on the substrates directly without any bottom electrodes or buffer layers, so it is easy to form an epitaxial thin film when the top material has the similar structure with the substrate. According to the Bragg diffraction equation, we can calculate the in- and out-of-plane lattice parameters *a* and *c*, showing in Table 1.

There are three factors that can influence the piezoelectricity of thin films. First, it is the crystal structure. Generally, the piezoelectricity of epitaxial thin film is better than the correspondingly polycrystalline one because of the anisotropy. The second one is the misfit strain between

Table 1
Calculated properties of the films on different substrates.

Substrate	a (Å)	c (Å)	V (Å^3)	S_M (10^{-3})	TEC (10^{-6} K^{-1})
LAO	3.944	3.994	62.127	−4.29	10
STO	3.945	3.975	61.863	−2.53	10.4
Si	3.937	3.951	61.240	-	2.6

thin films and substrates caused by the lattice parameters difference and/or the thermal expansion coefficient (TEC) mismatch between the substrate and the clamped thin film upon cooling. For epitaxial thin films, misfit strain (S_M) can be calculated as $S_M = {}^{(a-a_0)}/_{a_0}$, where a_0 is the unstrained cubic in-plane lattice parameter calculated by equation $a_0 = (a{\cdot}a{\cdot}c)^{1/3}$ (see Table 1). The negative S_M values indicate that films are under a compressive strain. The last factor is the microstructure of thin films, such as domain structure, grain size, grain destiny, surface roughness, etc., which can cause the diversity of piezoelectric properties. According to XRD patterns and previous research works, we can expect the piezoelectricity, both intrinsic piezoelectric response (led by lattice distortion) and the extrinsic piezoelectric activity (caused by domain wall motion) of KNLNS-BZ/LAO thin film is higher than KNLNS-BZ/Si thin film, and KNLNS-BZ/STO has moderate piezoelectricity considering the lower misfit strain (−0.00253) from 5° miscut substrate.

To characterize the microstructure of the thin films, DART-PFM was used and the results are shown in Fig. 2. It is clear that all the samples have smooth surfaces and the small triangle-like grains have the same size. So, it could be concluded that these three films have similar topography. Furthermore, the magnitude of PFM amplitude is related to the strength of piezoelectricity as they were scanned with the same driving bias. From Fig. 2 (middle column), the KNLNS-BZ/Si thin film has the largest response according to color bars, which might not be the intrinsic signal because of the frequency drift. Because the DART-PFM only excites two frequencies on both sides of resonance frequency, which is not reliable and stable for fitting the highly nonlinear equation of amplitude and frequency. This fitting is described as a simple harmonic oscillator (SHO) model shown below [21,29]. DART-PFM uses unstable amplitude signal to compare piezoelectricity between different samples, which may cause data deviation. The phase signal also shows the compelling diversity of three films. We can observe the nanodomain (black color parts) in both phase images of thin films grown on

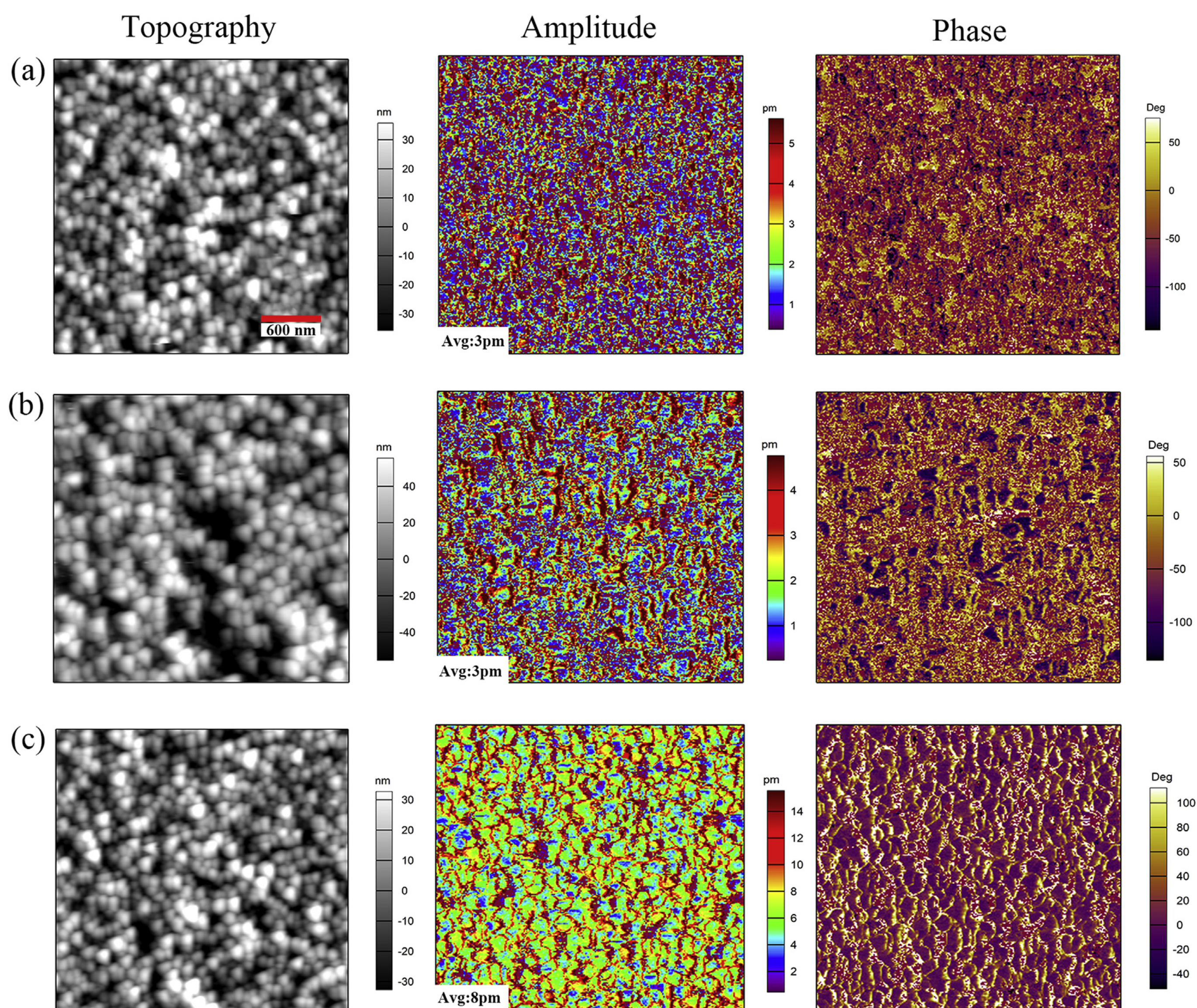

Fig. 2. DART-PFM images of topography, amplitude, and phase signal of KNLNS-BZ thin films grown on different substrates: (a) LAO; (b) STO; (c) Si. “Avg” is short for average, which is the mean value of the whole image.

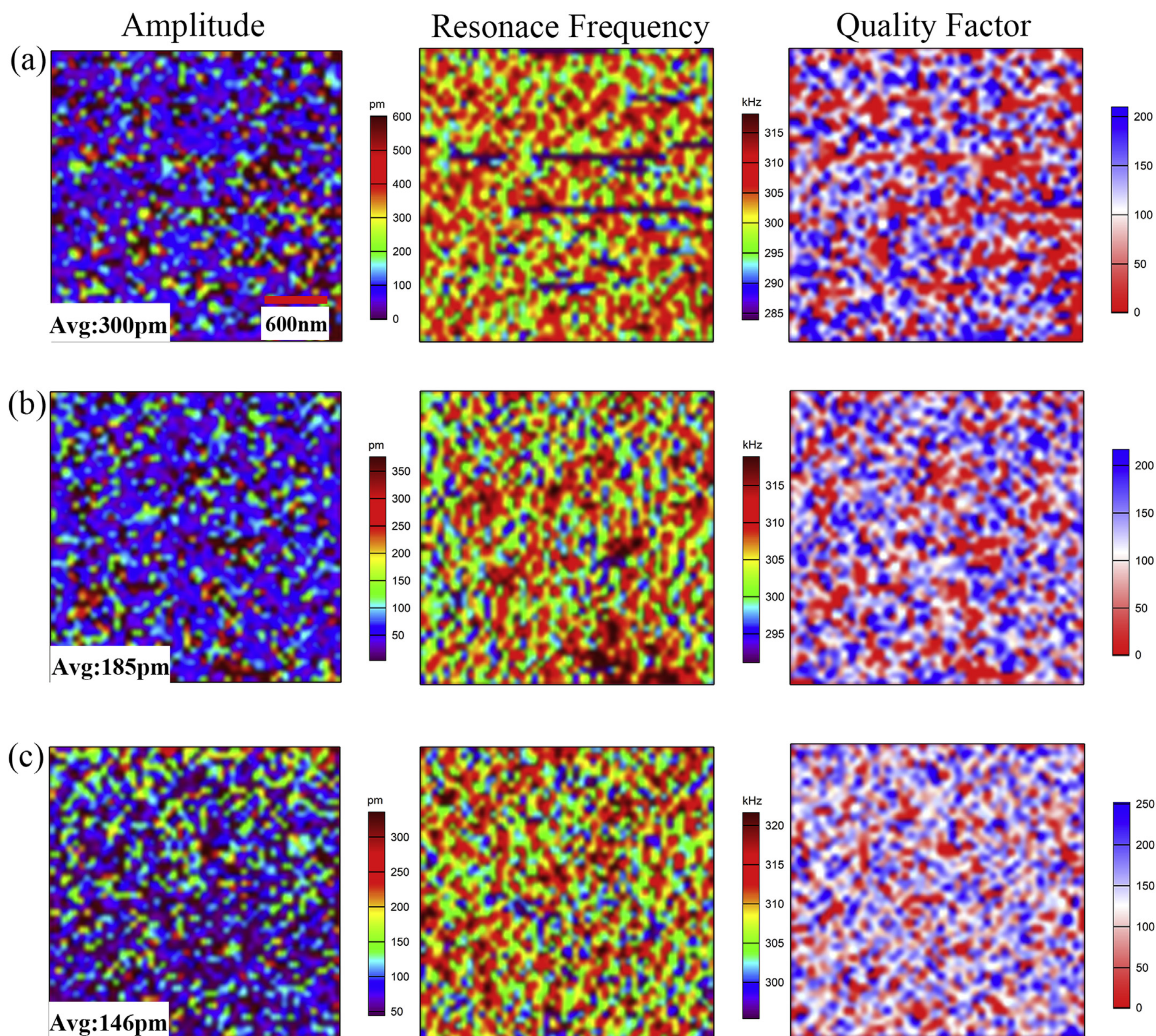

Fig. 3. Amplitude, quality factor (Q) and resonance frequency acquired by BE-PFM: (a) KNLNS-BZ/LAO; (b) KNLNS-BZ/STO; (c) KNLNS-BZ/Si. "Avg" is short for average, which is the mean value of the whole image.

perovskite single crystals. Nanodomain in the film grown on LAO substrate is smaller than the one on STO, which means more domain walls. It does not show clear domain signal in the out-of-plane direction from the polycrystalline film grown on Si substrate.

To solve the problem from DART-PFM and measure piezoresponse excluding the factor from frequency shifting, BE-PFM has been adopted. This method simultaneously excites and detects within a band of frequencies over a selected frequency range (usually covers the resonance frequency) to ensure that it's able to acquire the resonance signal during the full measurement process [22–24]. The cantilever's response is measured and has been Fourier transformed, and the generating amplitude– and phase–frequency curves will be stored as a 3D (collecting A(ω) and ϕ(ω) data at each point) data set. The data set will be fitted by SHO model, which can describe the dynamics of the interaction between a cantilever with a sharp tip and the sample surface well. The model is shown below, in (1) and (2), where A_0, ω_0, and Q are intrinsic electromechanical response (piezoelectricity), resonance frequency (elasticity), and quality factor (energy dissipation of the system that we are interested in determining quantitatively from the PFM experiment), respectively [21,29]. Data fitting of the piezoresponse peak at the resonance frequency is guaranteed.

$$\mathrm{A}(\omega) = \frac{A_0\omega_0^2}{\sqrt{(\omega^2-\omega_0^2)^2+\left(\frac{\omega_0\omega}{Q}\right)^2}} \tag{1}$$

$$\tan(\phi(\omega)) = \frac{\omega\omega_0/Q}{\omega^2-\omega_0^2} \tag{2}$$

We scanned 50 × 50 grid points in a 3 μm × 3 μm region using BE-PFM and then fitted through SHO model, the results are shown in Fig. 3. The average amplitudes of KNLNS-BZ/LAO, KNLNS-BZ/STO, and KNLNS-BZ/Si are 300 pm, 185 pm, and 146 pm, respectively. As mentioned, the amplitude refers to the piezoresponse ability, so it could tell that the piezoelectricity of KNLNS-BZ/LAO is about double of those of KNLNS-BZ/STO and KNLNS-BZ/Si. It is noticed that miscut substrate has a significant effect on the piezoelectricity of thin film. Moreover,

Fig. 4. Intrinsic amplitude, resonance frequency and quality factor (Q) acquired by SE-PFM; (a) KNLNS-BZ/LAO; (b) KNLNS-BZ/STO; (c) KNLNS-BZ/Si. "Avg" is short for average, which is the mean value of the whole image.

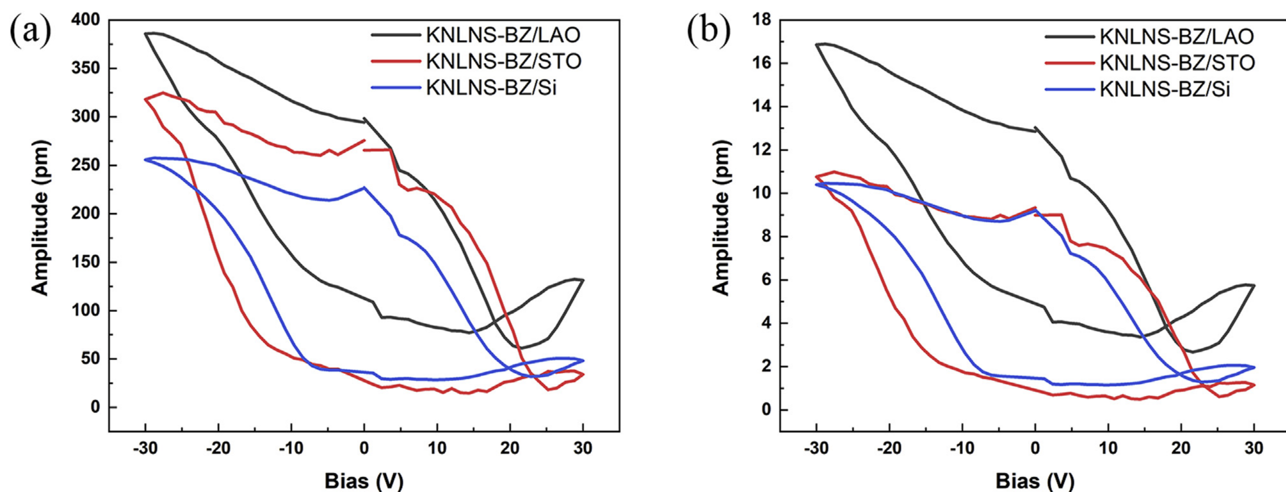

Fig. 5. Representative local PFM amplitude hysteresis loops (usually called "Butterfly-loop"): (a) direct measurement results; (b) intrinsic amplitude hysteresis loops deducted amplification from instrument.

Table 2
Coercive voltages and imprint voltages of the three films.

	V_p (V)	V_n (V)	V_i (V)	V_c (V)
KNLNS-BZ/LAO	21.6	14.4	3.6	18
KNLNS-BZ/STO	25.2	14.4	5.4	19.8
KNLNS-BZ/Si	22.8	9.6	6.6	16.2

resonance frequency representing elasticity and quality factor referring to energy dissipation of the three films are similar, which means that different substrates did not affect their elasticity and energy dissipation.

Although BE-PFM is a good solution to guarantee the signal stability, it excites a band of frequency simultaneously with constant excitation energy, which reduces its signal strength and causes the poor-data quality. This is obvious in Fig. 3, where all images have a low signal-to-noise ratio (SNR) and does not show strong detailed features. The most important deficiency in Fig. 3 is that we still did not obtain accurate piezoelectric coefficients from three samples, even we knew KNLNS-BZ/LAO has the highest piezoresponse. In fact, according to Equation (1), the amplitude we acquired in BE-PFM is $A_0{\cdot}Q$, an amplified signal. Though we can calculate A_0 using the average amplitude and average quality factor obtained from the images, which is 2.857 pm, 1.703 pm and 1.160 pm, respectively, this will increase error considering the divergence of every point. A new PFM method combining with machine learning called sequential excitation PFM (SE-PFM) developed by Jiangyu Li et al. may be helpful to measure piezoelectric coefficients [29]. Unlike BE-PFM, this method excites a frequency band near the resonance frequency as a function of time, which means it excites one frequency at a time, and changes excitation frequency at next time. This method can guarantee a strong signal and high SNR. With the help of unsupervised principle component analysis which speeds up physical analysis by at least four orders of magnitude and physics-based SHO analysis, the first three PCA components of three films can be seen in Supporting Information Figs. S1, S2, and S3 in which we can obtain intrinsic amplitude, resonance frequency and quality factor. As shown in Fig. 4, the average intrinsic amplitudes of KNLNS-BZ/LAO, KNLNS-BZ/STO, and KNLNS-BZ/Si are 2.5 pm, 1.3 pm, and 1.4 pm, respectively, while the amplitude only contains intrinsic piezoresponse original from lattice distortion. This result exhibits a similar proportion with BE-PFM. According to Table 1, we knew the misfit strain of three films can be ranked in a decreasing sequence of KNLNS-BZ/LAO, KNLNS-BZ/STO, and KNLNS-BZ/Si, representing the same tendency of lattice distortion. However, Fig. 4 shows that piezoresponse of KNLNS-BZ/Si is a little larger than that of KNLNS-BZ/STO. When considering the composite effect of lattice distortion caused by the polycrystalline thin film on Si substrate and the reduction of amplitude in the direction of out of plane caused by the slope of miscut STO substrate, they are quite close.

Amplitude hysteresis loops, a typical way to compare the piezoelectricity at the nanoscale, are shown in Fig. 5 to confirm our previous hypothesis. The largest amplitudes of KNLNS-BZ/LAO, KNLNS-BZ/STO, and KNLNS-BZ/Si are 17 pm, 10.8 pm, and 10.1 pm, respectively. So the calculated values of d_{33} are 21.25 pm/V, 13.5 pm/V, and 12.625 pm/V, respectively. The d_{33} value of the film grown on LAO is higher than the reported valued of epitaxial $PbZr_{0.2}Ti_{0.8}O_3$ thin film (d_{33} = 19 ± 1 pm/V) [34]. Obviously, a similar proportion appeared again along with SE-PFM results. The only difference is that d_{33} of KNLNS-BZ/STO appears higher than that of KNLNS-BZ/Si. This is because SS-PFM measured both intrinsic and extrinsic piezoresponse signal. As reported in Fig. 2, KNLNS-BZ/STO has more nanodomains than KNLNS-BZ/Si, so it showed higher piezoresponse when we considered external effect. What's more, we can also acquire coercive voltages and imprint voltages from hysteresis loops, as shown in Table 2. V_p is positive voltage, V_n is negative voltage, V_i is imprint voltage, and V_c is coercive voltage, while V_i and V_c are calculated from V_p and V_n as formula showed below (3,4). Epitaxial films have larger coercive voltage than polycrystalline one.

$$V_i = \frac{|V_p| - |V_n|}{2} \tag{3}$$

$$V_c = \frac{|V_p| + |V_n|}{2} \tag{4}$$

As we have adopted and practiced several PFM methods, the advantages and disadvantages of each method are summarized in Table 3. DART-PFM, BE-PFM, SE-PFM all have their own advantages can meet certain experimental requirements.

After studying the crystal structures and local piezoelectric properties of thin films on different substrates carefully, we can build up the relationship between structure and property. The intrinsic piezoelectric response is mostly influenced by lattice distortion and extrinsic piezoelectric activity is dominated by domain wall motion. In our research, lattice distortion is affected by misfit strain, which is mostly caused by the lattice parameters mismatch and the differences in thermal expansion coefficients between substrates and the clamped thin films. Piezoelectric activity is also influenced by the orientation of films, so we find out that intrinsic piezoelectricity of well epitaxial thin film is the highest and nearly double of the remnant two.

4. Conclusion

In this work, we adopted several PFM methods (DART-PFM, BE-PFM, SE-PFM, etc.) to continuously approach accurately piezoelectric coefficients of KNLNS-BZ thin film. With the great help of machine learning we can build up the local structure-property relationship of piezoelectric thin films. These results clearly showed that the influence from substrates: the piezoelectricity of epitaxial KNLNS-BZ thin film on LAO (21.25 pm/V) is nearly double of the one on Si.

Table 3
Comparison of different PFM measurement methods.

	Advantages	Disadvantages	Scope of application
DART-PFM	1 Can acquire clear morphology, amplitude and phase directly and simultaneously 2 Very fast to acquire data (~2 min)	Cannot measure quantitatively because of amplification from instrument and frequency drift	To measure morphology, piezoelectricity, domain
BE-PFM	1 Can obtain amplitude, phase, resonance frequency and quality factor 2 Relatively fast to obtain data (~30 min) 3 Relative quantitative	1.SNR is too low to show the detailed features 2.Data is amplified	To quickly measure piezoelectricity including both intrinsic and extrinsic, elasticity and energy dissipation semiquantitatively
SE-PFM	1 Can obtain intrinsic amplitude, resonance frequency and quality factor 2 Quantitative 3 High SNR	1.Pretty slow to gain data (~3 h) 2.Cannot obtain phase accurately	To measure intrinsic piezoelectricity, elasticity and energy dissipation quantitatively

Declaration of competing interest

The authors declare that they have no known competing financial interests or personal relationships that could have appeared to influence the work reported in this paper.

Acknowledgements

This work was supported by the National Key R&D Program of China (2017YFA0208000), National Science Foundation of China (Grant No. 51831010, 51621063), Program for Changjiang Scholars and Innovative Research Team in University (IRT_17R85) and the Fundamental Research Funds for the Central Universities (xtr0118016). We appreciate for Yanshuang Hao for providing KNLNS-BZ ceramic as the PLD target, and also thanks for the useful suggestions and language improvements from Dawei Zhang and Ahsan Ali.

Appendix A. Supplementary data

Supplementary data to this article can be found online at https://doi.org/10.1016/j.ceramint.2019.12.174.

References

[1] R. Guo, L.E. Cross, S.-E. Park, B. Noheda, D.E. Cox, G. Shirane, Origin of the high piezoelectric response in $PbZr_{1-x}Ti_xO_3$, Phys. Rev. Lett. 84 (2000) 5423–5426.
[2] W. Jo, R. Dittmer, M. Acosta, J. Zang, C. Groh, E. Sapper, K. Wang, J. Rödel, Giant electric-field-induced strains in lead-free ceramics for actuator applications – status and perspective, J. Electroceram. 29 (2012) 71–93.
[3] C. Li, L. Wang, W. Chen, L. Lu, H. Nan, D. Wang, Y. Zhang, Y. Yang, C.-L. Jia, A novel multiple interface structure with the segregation of dopants in lead-free ferroelectric $(K_{0.5}Na_{0.5})NbO_3$ thin films, Adv. Mater. Interfaces 5 (2018) 1700972.
[4] J.A. Rodriguez, A. Etxeberria, L. González, A. Maiti, Structural and electronic properties of $PbTiO_3$, $PbZrO_3$, and $PbZr_{0.5}Ti_{0.5}O_3$: first-principles density-functional studies, J. Chem. Phys. 117 (2002) 2699–2709.
[5] D. Pantel, S. Goetze, D. Hesse, M. Alexe, Room-temperature ferroelectric resistive switching in ultrathin $Pb(Zr_{0.2}Ti_{0.8})O_3$ Films, ACS Nano 5 (2011) 6032–6038.
[6] I.K. Bdikin, J.A. Pérez, I. Coondoo, A.M.R. Senos, P.Q. Mantas, A.L. Kholkin, Ferroelectric domain structure of $PbZr_{0.35}Ti_{0.65}O_3$ single crystals by piezoresponse force microscopy, J. Appl. Phys. 110 (2011) 052003.
[7] H.J. Seog, A. Ullah, C.W. Ahn, I.W. Kim, S.Y. Lee, J. Park, H.J. Lee, S.S. Won, S.-H. Kim, Recent progress in potassium sodium niobate lead-free thin films, J. Korean Phys. Soc. 72 (2018) 1467–1483.
[8] Y. Saito, H. Takao, T. Tani, T. Nonoyama, K. Takatori, T. Homma, T. Nagaya, M. Nakamura, Lead-free piezoceramics, Nature 432 (2004) 84–87.
[9] J. Rödel, W. Jo, K.T.P. Seifert, E.-M. Anton, T. Granzow, D. Damjanovic, Perspective on the development of lead-free piezoceramics, J. Am. Ceram. Soc. 92 (2009) 1153–1177.
[10] J.-F. Li, K. Wang, F.-Y. Zhu, L.-Q. Cheng, F.-Z. Yao, D.J. Green, (K,Na)NbO3-based lead-free piezoceramics: fundamental aspects, processing technologies, and remaining challenges, J. Am. Ceram. Soc. 96 (2013) 3677–3696.
[11] J. Luo, W. Sun, Z. Zhou, Y. Bai, Z.J. Wang, G. Tian, D. Chen, X. Gao, F. Zhu, J.F. Li, Domain evolution and piezoelectric response across thermotropic phase boundary in $(K,Na)NbO_3$-based epitaxial thin films, ACS Appl. Mater. Interfaces 9 (2017) 13315–13322.
[12] H.M. HL, E. Martinez-Aguilar, J.J. Gervacio-Arciniega, X. Vendrell, J.M. Siqueiros-Beltrones, O. Raymond-Herrera, Structure and piezo-ferroelectricity relationship study of $(K_{0.5}Na_{0.5})_{0.985}La_{0.005}NbO_3$ epitaxial films deposited on $SrTiO_3$ by sputtering, Sci. Rep. 7 (2017) 17721.
[13] S. Zhang, R. Xia, T.R. Shrout, Modified $(K_{0.5}Na_{0.5})NbO_3$ based lead-free piezoelectrics with broad temperature usage range, Appl. Phys. Lett. 91 (2007) 132913.
[14] K. Wang, J.-F. Li, Domain engineering of lead-free Li-modified $(K,Na)NbO_3$ polycrystals with highly enhanced piezoelectricity, Adv. Funct. Mater. 20 (2010) 1924–1929.
[15] M.D. Nguyen, M. Dekkers, E. Houwman, R. Steenwelle, X. Wan, A. Roelofs, T. Schmitz-Kempen, G. Rijnders, Misfit strain dependence of ferroelectric and piezoelectric properties of clamped (001) epitaxial $Pb(Zr_{0.52},Ti_{0.48})O_3$ thin films, Appl. Phys. Lett. 99 (2011) 252904.
[16] C. Li, L. Wang, Z. Wang, Y. Yang, W. Ren, G. Yang, Atomic resolution interfacial structure of lead-free ferroelectric $K_{0.5}Na_{0.5}NbO_3$ thin films deposited on $SrTiO_3$, Sci. Rep. 6 (2016) 37788.
[17] W. Zhang, H. Zhang, J. Ouyang, F. Hu, Effects of elastic coupling between $BaTiO_3$ ferroelectric film and a substrate with finite thickness on piezoelectric coefficients, Acta Phys. Pol. 131 (2017) 1426–1430.
[18] J.X. Zhang, D.G. Schlom, L.Q. Chen, C.B. Eom, Tuning the remanent polarization of epitaxial ferroelectric thin films with strain, Appl. Phys. Lett. 95 (2009) 122904.
[19] C. Cui, F. Xue, W.-J. Hu, L.-J. Li, Two-dimensional materials with piezoelectric and ferroelectric functionalities, npj 2D Mater. Appl. 2 (2018) 18.
[20] B.J. Rodriguez, C. Callahan, S.V. Kalinin, R. Proksch, Dual-frequency resonance-tracking atomic force microscopy, Nanotechnology 18 (2007) 470054.
[21] A. Gannepalli, D.G. Yablon, A.H. Tsou, R. Proksch, Mapping nanoscale elasticity and dissipation using dual frequency contact resonance AFM, Nanotechnology 22 (2011) 355705.
[22] S. Jesse, S.V. Kalinin, R. Proksch, A.P. Baddorf, B.J. Rodriguez, The band excitation method in scanning probe microscopy for rapid mapping of energy dissipation on the nanoscale, Nanotechnology 18 (2007) 435503.
[23] S. Jesse, S.V. Kalinin, Band excitation in scanning probe microscopy: sines of change, J. Phys. D Appl. Phys. 44 (2011) 464006.
[24] S. Jesse, R.K. Vasudevan, L. Collins, E. Strelcov, M.B. Okatan, A. Belianinov, A.P. Baddorf, R. Proksch, S.V. Kalinin, Band excitation in scanning probe microscopy: recognition and functional imaging, Annu. Rev. Phys. Chem. 65 (2014) 519–536.
[25] L. Li, Y. Cao, S. Somnath, Y. Yang, S. Jesse, Y. Ehara, H. Funakubo, L.-Q. Chen, S.V. Kalinin, R.K. Vasudevan, Direct imaging of the relaxation of individual ferroelectric interfaces in a tensile-strained film, Adv. Electron. Mater. 3 (2017) 1600508.
[26] J.C. Agar, Y. Cao, B. Naul, S. Pandya, S. van der Walt, A.I. Luo, J.T. Maher, N. Balke, S. Jesse, S.V. Kalinin, R.K. Vasudevan, L.W. Martin, Machine detection of enhanced electromechanical energy conversion in $PbZr_{0.2}Ti_{0.8}O_3$ thin films, Adv. Mater. 30 (2018) 1800701.
[27] L. Li, Y. Yang, D. Zhang, Z.-G. Ye, S. Jesse, S.V. Kalinin, R.K. Vasudevan, Machine learning–enabled identification of material phase transitions based on experimental data: exploring collective dynamics in ferroelectric relaxors, Sci. Adv. 4 (2018) eaap8672.
[28] H. Trivedi, V.V. Shvartsman, M.S.A. Medeiros, R.C. Pullar, D.C. Lupascu, Sequential piezoresponse force microscopy and the 'small-data' problem, npj Comput. Mater. 4 (2018) 28.
[29] B. Huang, E.N. Esfahani, J. Li, Mapping intrinsic electromechanical responses at the nanoscale via sequential excitation scanning probe microscopy empowered by deep data, Natl. Sci. Rev. 6 (2019) 55–63.
[30] Q. Li, C.T. Nelson, S.L. Hsu, A.R. Damodaran, L.L. Li, A.K. Yadav, M. McCarter, L.W. Martin, R. Ramesh, S.V. Kalinin, Quantification of flexoelectricity in $PbTiO_3$/$SrTiO_3$ superlattice polar vortices using machine learning and phase-field modeling, Nat. Commun. 8 (2017) 1468.
[31] B. Zhang, J. Wu, X. Cheng, X. Wang, D. Xiao, J. Zhu, X. Wang, X. Lou, Lead-free piezoelectrics based on potassium-sodium niobate with giant d_{33}, ACS Appl. Mater. Interfaces 5 (2013) 7718–7725.
[32] J. Gao, S. Ren, L. Zhang, Y. Hao, M. Fang, M. Zhang, Y. Dai, X. Hu, D. Wang, L. Zhong, S. Li, X. Ren, Phase transition sequence in Pb-free $0.96(K_{0.5}Na_{0.5})_{0.95}Li_{0.05}Nb_{0.93}Sb_{0.07}O_3-0.04BaZrO_3$ ceramic with large piezoelectric response, Appl. Phys. Lett. 107 (2015) 032902.
[33] I.Y. Abdullah, M. Yahaya, M.H.H.J. Jumali, H.M. Shanshool, Enhancement piezoelectricity in poly(vinylidene fluoride) by filler piezoceramics lead-free potassium sodium niobate (KNN), Opt. Quant. Electron. 48 (2016) 149.
[34] J. Song, Z. Xiao, B. Chen, S. Prockish, X. Chen, A. Rajapitamahuni, L. Zhang, J. Huang, X. Hong, Enhanced piezoelectric response in hybrid lead halide perovskite thin films via interfacing with ferroelectric $PbZr_{0.2}Ti_{0.8}O_3$, ACS Appl. Mater. Interfaces 10 (2018) 19218–19225.